

Supporting Information

Lew et al. 10.1073/pnas.1114444108

SI Text

Double-Helix Point Spread Function (DH-PSF) Automated Recognition and Fitting. The 3D locations of single molecules are extracted frame-by-frame from raw movies using an automated image-processing algorithm implemented in MATLAB. This algorithm contains two components: (i) a coarse recognition step, in which DH-PSFs are identified and localized with integer-pixel resolution, and (ii) a fine fitting stage, which fits each DH-PSF image identified above to a double-Gaussian model of the DH-PSF and produces 3D positions. The algorithm can fit approximately 15–20 molecules per second on an Intel Core 2 Duo workstation with 4 GB of RAM.

The coarse recognition algorithm uses template matching to identify DH-PSFs from raw data containing single molecules. Template matching is a process in which instances of a known template $t(x,y)$ are identified in an image $s(x,y)$ by selecting locations (p, q) that minimize the mean-squared error quantity

$$E(p,q) = \sum_x \sum_y [s(x,y) - t(x-p,y-q)]^2.$$

The minimization of the error quantity may be equivalently recast as the maximization of the area correlation, $r(p,q) = s(p,q) \otimes t(-p, -q)$. Because the convolution operation is computationally costly, this operation is performed in the Fourier domain as a simple multiplication.

Because the DH-PSF rotates as a function of the axial position of an emitter, several templates must be used to recognize all possible orientations of the DH-PSF. The templates used in the detection algorithm are taken from the fluorescent bead calibration movies measured at the same imaging conditions as the single-molecule data. Five templates were chosen, with the DH-PSF rotated approximately 30 degrees between each template (see Fig. S4). This number of templates represents a good balance between matching accuracy and computational speed.

Template matching with each of the templates is performed using phase correlation in the Fourier domain. Phase correlation normalizes the input image and template image amplitudes in the Fourier domain, thereby minimizing the bias of template matching to bright regions of the image. Before transforming to the Fourier domain, each template t_k is padded with zeros to match the size of the raw data. The phase correlation image r_k is then computed from the raw data s and the k th template with the formula

$$r_k = F^{-1} \left(\frac{F\{h\}F\{s\}F\{t_k\}^*}{|F\{s\}||F\{t_k\}|} \right),$$

where F denotes the two-dimensional Fourier transform, F^{-1} denotes the two-dimensional inverse Fourier transform, and the prefilter h is a Gaussian low pass filter with a width $\sigma = 1.5$ pixels. Because phase correlation emphasizes high frequency components (1) and these spatial frequencies typically have a lower signal to background ratio, the Gaussian low pass filter h is used to filter out these higher frequencies and thus leads to more robust template matches.

Local maxima (i.e., peaks) above a user-defined threshold are detected in each image r_k , and the locations and magnitudes of each peak are stored in memory. Because the peak threshold is set low enough to detect weak single molecules, extraneous matches occur for brighter single molecules. If the candidate DH-PSF is bright enough, a template will match at locations

where only one of its spots overlaps with only one of the spots in the input image. These ghost matches are filtered out by enforcing a minimum distance between all of the template matches in a given frame of the input data. This minimum distance is chosen to be the typical diameter of the DH-PSF image (1.2 μm). If multiple template matches occur too close to one another, the strongest match is chosen, and the others are discarded. A raw fluorescence image of single-molecule PAINT using Nile red is shown in Fig. S5A. DH-PSFs identified by the template matching code are circled in the image.

Once template matching has computed the location of single molecules to integer-pixel precision, these locations are processed by a double Gaussian-fitting algorithm to extract 3D superresolution information. The MATLAB optimization function `lsqnonlin` is used to minimize the mean-square difference between the input data and an eight-parameter double Gaussian model $f(x,y)$ of the DH-PSF, given by

$$f(x,y) = \hat{A}_1 \exp\left\{\frac{-[(x-\hat{x}_1)^2 + (y-\hat{y}_1)^2]}{2\hat{\sigma}_1^2}\right\} + \hat{A}_2 \exp\left\{\frac{-[(x-\hat{x}_2)^2 + (y-\hat{y}_2)^2]}{2\hat{\sigma}_2^2}\right\} + B.$$

Four parameters are used for each Gaussian function: amplitude (\hat{A}_1 and \hat{A}_2), x -center location (\hat{x}_1 and \hat{x}_2), y -center location (\hat{y}_1 and \hat{y}_2), and width ($\hat{\sigma}_1$ and $\hat{\sigma}_2$). The constant offset B is computed from the mean fluorescence background hand-designated in each image. Although this double Gaussian model is only an approximation of the true shape of the DH-PSF (2, 3), it represents a good compromise between fitting accuracy and computational complexity. These fits are then filtered to ensure that they match the data sufficiently accurately and produce good reconstructions of the DH-PSF [i.e., positive amplitudes for both \hat{A}_1 and \hat{A}_2 , an \hat{A}_1/\hat{A}_2 ratio near unity, values of $\hat{\sigma}_1$ and $\hat{\sigma}_2$ between 60 and 180 nm (characteristic sizes of the DH-PSF), etc.].

For the raw fluorescence image shown in Fig. S5A, a reconstruction of all successfully fitted DH-PSFs is shown in Fig. S5B. Eight of the nine DH-PSFs identified by the template matching code were successfully fitted to double Gaussians, validating the code's ability to recognize and fit images of the DH-PSF. This algorithm facilitates the processing of hundreds of thousands of localizations in an efficient and timely manner.

The midpoint between the two fitted Gaussians yields the x and y location of the localized single molecule, whereas the angle between the two Gaussians can be converted into a z position using a calibration curve (see Fig. 1C). Because of aberrations in the $4f$ imaging system, the DH-PSF also slightly translates laterally as a function of the z position of the emitter (3). This effect was removed by measuring the lateral translation of a fluorescent bead as it was scanned along the axial direction (Fig. S6).

Drift Characterization. For superresolution by power-dependent active intermittency and points accumulation for imaging in nanoscale topography (SPRAIPAIN) imaging, the translation of two to three fiducial fluorescent beads were averaged together to track the drift of the microscope stage in time. This measurement is essential for an extended superresolution imaging experiment, as the typical drift of the microscope stage is on the order of hundreds of nanometers. Fig. S7 shows the typical drift measured during a SPRAIPAIN imaging experiment. Overall, the drift

in the y direction is the worst of the three directions but can easily be corrected because of the high precision with which the fiducials are localized (Fig. S7, *Inset*).

Calculation of Localization Precision. The localization precision of each measurement was computed from the previously measured scaling law (2)

$$\sigma_x = \left(\frac{410}{N_{\text{eq}}}\right)^{0.47}, \quad \sigma_y = \left(\frac{550}{N_{\text{eq}}}\right)^{0.52}, \quad \sigma_z = \left(\frac{830}{N_{\text{eq}}}\right)^{0.49},$$

where N is the number of photons detected, B is the measured background per pixel, and $N_{\text{eq}} = 1.5N/\sqrt{B}$ normalizes the difference in background shot noise between our measurements and ref. 2. These equations give a reasonable estimate of the localization precision, because the dominant source of noise in our experiments is photon shot noise.

Calculation of the Cell's Central Axis. The location of each cell's central axis was computed using a custom script written in

1. Brunelli R (2009) *Template Matching Techniques in Computer Vision: Theory and Practice* (Wiley, Chichester, U.K.), p 338.
2. Thompson MA, Lew MD, Badieirostami M, Moerner WE (2010) Localizing and tracking single nanoscale emitters in three dimensions with high spatiotemporal resolution using a double-helix point spread function. *Nano Lett* 10:211–218.

MATLAB. The algorithm works as follows: (i) PAINT localizations from a single cell were rotated in 3D space so that they were aligned with the x axis as closely as possible; (ii) the localizations were partitioned into slices along the x axis (300-nm thick, 100-nm sampling). The thickness and sampling interval for the slices were chosen to ensure that the resulting central axis was smooth. For each slice k , the best center transverse location ($y_{\text{ck}}, z_{\text{ck}}$) was computed by minimizing the standard deviation of the squared distance between the best center location and each localization, given by

$$s_k(y_{\text{ck}}, z_{\text{ck}}) = \sqrt{\frac{1}{N_k - 1} \sum_{i=1}^{N_k} (y_i - y_{\text{ck}})^2 + (z_i - z_{\text{ck}})^2},$$

where y_i, z_i is the transverse position of the i th localization and N_k is the number of localizations in slice k . The aforementioned quantity was minimized by using the MATLAB optimization function `lsqnonlin`. When plotting the cell's central axis, these locations were linearly interpolated.

3. Lew MD, Thompson MA, Badieirostami M, Moerner WE (2010) In vivo three-dimensional superresolution fluorescence tracking using a double-helix point spread function. *Proc SPIE* 7571:75710Z.

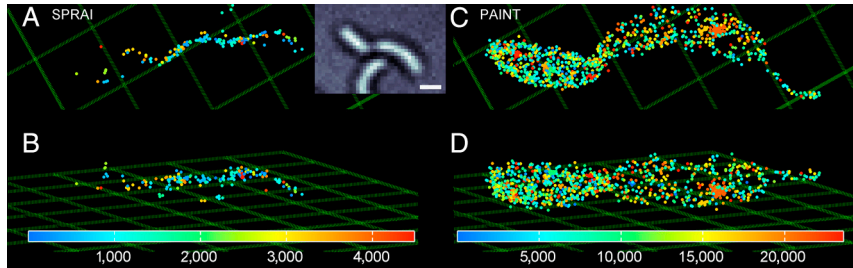


Fig. S1. Localization patterns versus time during SPRAIPAIN data acquisition. (A) The xy projection of localizations on a Crescentin-enhanced YFP (CreS-eYFP) fiber acquired from 4,732 frames of SPRAI imaging. *Inset* shows a transmission white-light image of the same field of view as A. (B) Three-dimensional projection of the fiber shown in A. (C) The xy projection of PAINT localizations of a *Caulobacter crescentus* cell membrane acquired from 23,582 frames of PAINT imaging. (D) Three-dimensional projection of the membrane shown in C. Grid and scale bar, 1 μm . Color bars in units of frames.

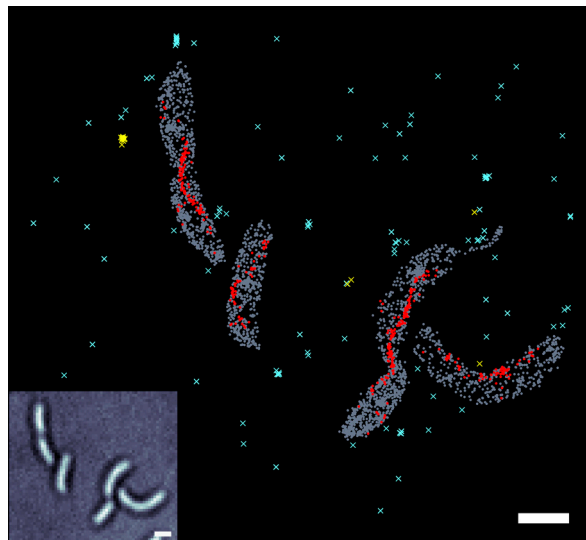


Fig. S2. Analysis of false positive rate of localization for 3D SPRAIPAIN. True SPRAI localizations of Crescentin-enhanced YFP (CreS-eYFP) are shown as red circles; false localizations are shown as yellow \times . True PAINT localizations of the cell membrane are shown as gray circles; false localizations are shown as cyan \times . *Inset* shows a transmission white-light image of the same field of view. Scale bars, 1 μm .

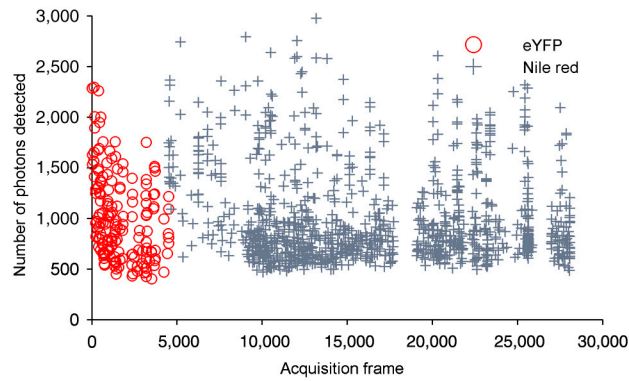


Fig. S3. Number of photons detected per localization versus acquisition time during SPRAIPAIN imaging. Enhanced YFP localizations were acquired during the first 4,499 frames, and the following 23,582 frames were used to collect Nile red localizations. Enhanced YFP localizations are shown as red circles; Nile red localizations are shown as grey crosses.

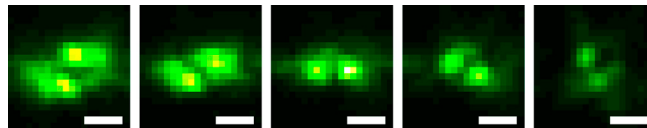


Fig. S4. Templates of the DH-PSF used by the automated template-matching algorithm. These images were taken from a 100-nm fluorescent bead in agarose gel at various z positions. Scale bars, 1 μm .

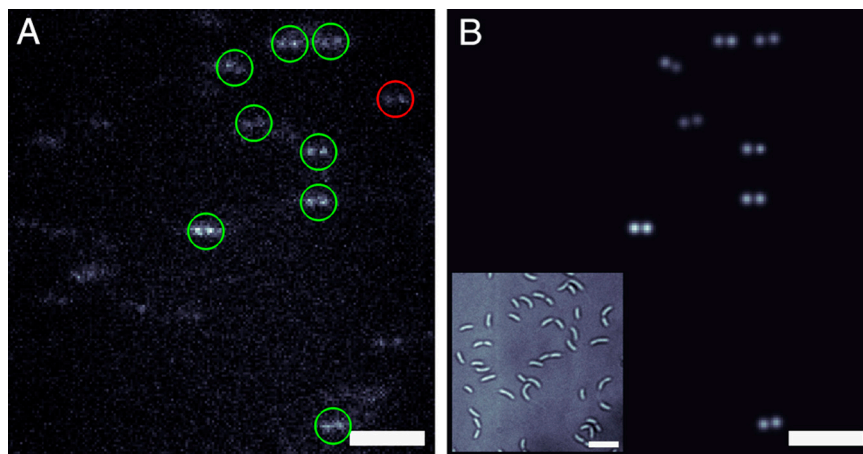


Fig. S5. Validation of the DH-PSF automated recognition and fitting algorithm. (A) Raw fluorescence image of Nile red labeling the cell membranes of *Caulobacter crescentus*. Circles are drawn around DH-PSFs that have been identified by the template-matching algorithm. Successful fits to a double-Gaussian function are shown in green; one unsuccessful fit is in red. (B) Reconstructed image of the successfully fitted DH-PSFs from A. Inset shows a white light transmission image of the same field of view. Scale bars, 5 μm .

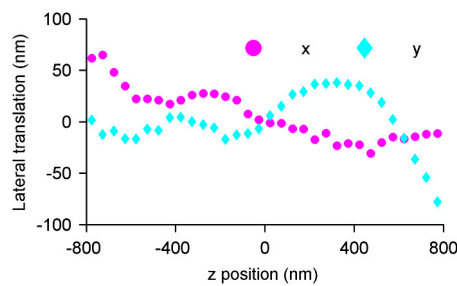


Fig. S6. Lateral translation of the DH-PSF as a function of the z position of an emitter. Translation in the x direction (magenta circles) and y direction (cyan diamonds) is shown over a 1.6- μm depth of field.

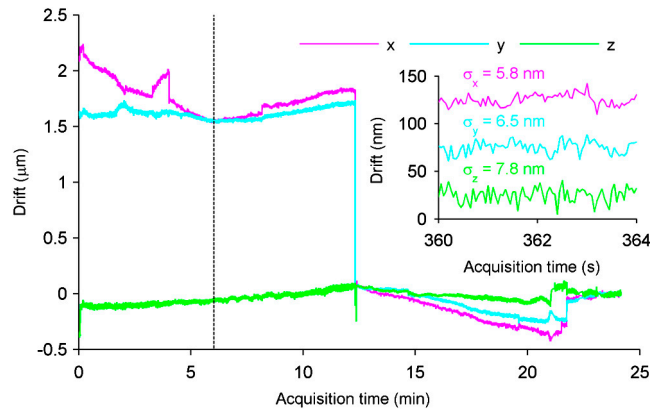
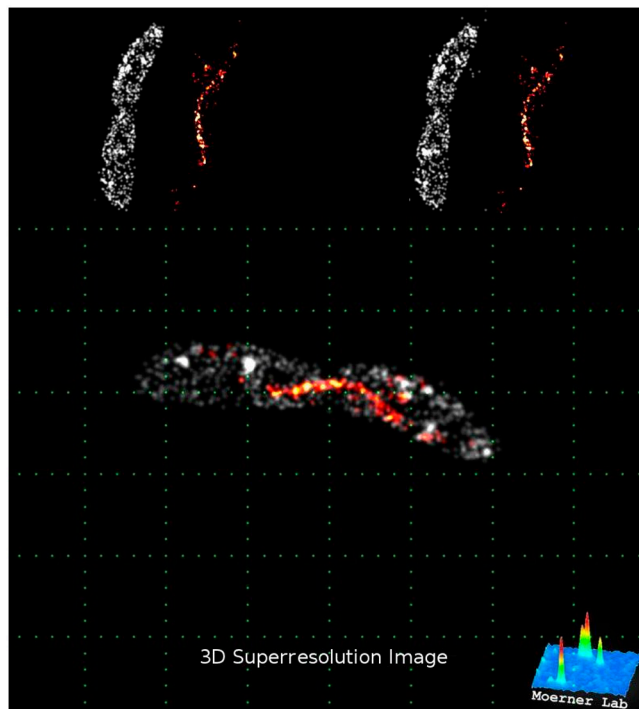
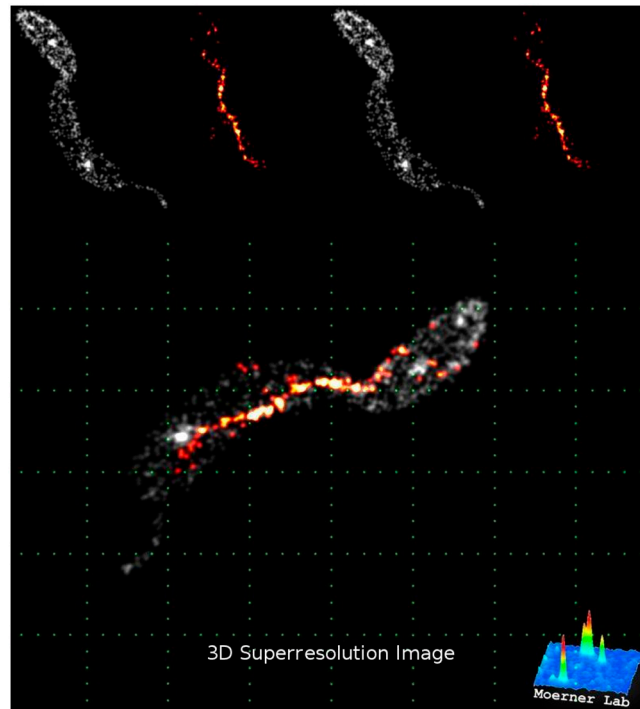


Fig. S7. Typical microscope stage drift during a SPRAIPAINT imaging experiment. The drift in x (magenta), y (cyan), and z (green) is shown for an approximately 25 min acquisition (eight 5,000-frame movies). *Inset* shows a 4-s track of the stage drift (comprising 81 localizations) acquired six minutes into the experiment (black dashed line). Standard deviations of these curves show a localization precision of 5.8 nm in the x direction, 6.5 nm in the y direction, and 7.8 nm in the z direction. The large 2- μm translation in x and y at approximately 12 min is due to administering the PAINT dye and switching band-pass filters in the microscope. The shift at approximately 21 min is due to a manual adjustment of the microscope stage.



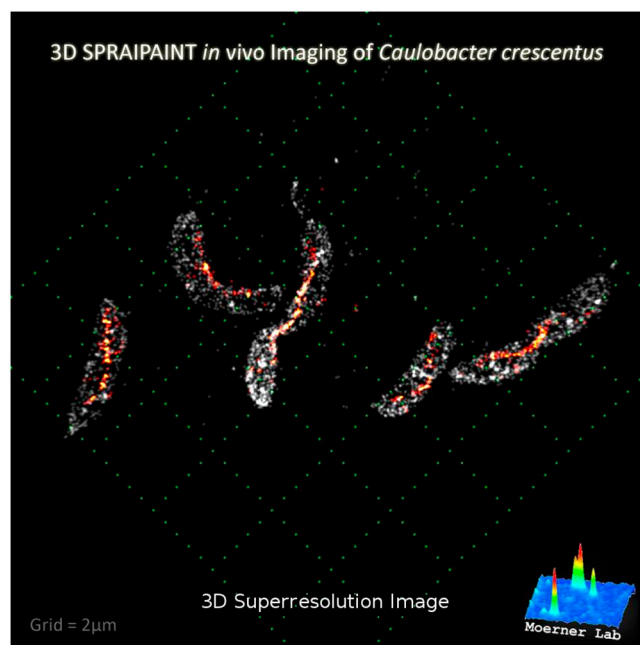
Movie S1. Three-dimensional SPRAIPAINT movie of a single isolated *Caulobacter crescentus* cell (Fig. 2 A–C). SPRAI: Enhanced YFP fused to Crescentin (CreS) is shown in red-yellow. PAINT: Nile red binding to the cellular surface is shown in gray. (*Upper*) Isometric projections of the cell separated into two color channels are shown revolving about both the x and y axes. (*Lower*) A revolving pinhole camera projection of the same cell showing 3D perspective. A 1- μm grid is shown in green for scale.

[Movie S1 \(WMV\)](#)



Movie S2. Three-dimensional SPRAIPAINT movie of another single isolated *Caulobacter crescentus* cell (Fig. 2 D–F). SPRAI: Enhanced YFP fused to Crescentin (CreS) is shown in red-yellow. PAINT: Nile red binding to the cellular surface is shown in gray. The stalk of the cell is clearly resolved. (*Upper*) Isometric projections of the cell separated into two color channels are shown revolving about both the x and y axes. (*Lower*) A revolving pinhole camera projection of the same cell showing 3D perspective. A 1- μ m grid is shown in green for scale.

[Movie S2 \(WMV\)](#)



Movie S3. Three-dimensional SPRAIPAINT movie of a large field of view ($10 \times 10 \mu\text{m}$, Fig. 2G) showing many cells imaged simultaneously. SPRAI: Enhanced YFP fused to Crescentin (CreS) is shown in red-yellow. PAINT: Nile red binding to the cellular surfaces is shown in gray. A 2- μ m grid is shown in green for scale.

[Movie S3 \(WMV\)](#)

